ACS APPLIED MATERIALS & INTERFACES

Research Article

www.acsami.org

Inkjet Fabrication of Copper Patterns for Flexible Electronics: Using Paper with Active Precoatings

Thomas Öhlund,*[,†] Anna K. Schuppert,[‡] Magnus Hummelgård,[†] Joakim Bäckström,[†] Hans-Erik Nilsson,[§] and Håkan Olin[†]

[†]Department of Natural Sciences, Mid Sweden University, SE-85170 Sundsvall, Sweden

[‡]Institut Charles Gerhardt de Montpellier - UMR 5253, 34095 Montpellier Cedex 5, France

[§]Department of Electronics Design, Mid Sweden University, SE-85170 Sundsvall, Sweden

Supporting Information

ABSTRACT: Low-cost solution-processing of highly conductive films is important for the expanding market of printed electronics. For roll-to-roll manufacturing, suitable flexible substrates and compatible postprocessing are essential. Here, custom-developed coated papers are demonstrated to facilitate the inkjet fabrication of high performance copper patterns. The patterns are fabricated in ambient conditions using water-based CuO dispersion and intense pulsed light (IPL) processing. Papers using a porous $CaCO_3$ precoating, combined with an acidic mesoporous absorption coating, improve the effectiveness and reliability of the IPL process. The processing is realizable within 5 ms, using a single pulse of light. A resistivity of 3.1 ± 0.12 $\mu\Omega$·cm is achieved with 400 μm wide conductors, corresponding to more than 50% of the conductivity of bulk copper. This is higher than previously reported results for IPL-processed copper.

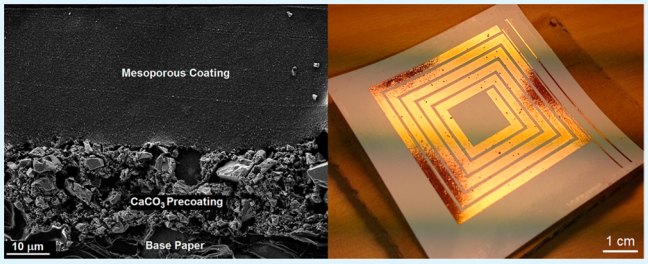

KEYWORDS: *intense pulsed light sintering, flash light sintering, printed flexible electronics, inkjet printing, paper coatings, copper patterns, IPL sintering, IPL processing*

1. INTRODUCTION

Printed electronics is an emerging manufacturing technology that has gained considerable interest in recent years. Reductions in cost and energy consumption, as well as less material waste, are important driving forces. In addition, the possibility to utilize low-cost flexible substrates and roll-to-roll manufacturing, further increases the competitiveness and potential application range. Electrically conducting thin films are important because they are fundamental parts of most printed circuits and devices such as conductive tracks,[1] antennas[2] and electrodes for sensors,[3] light-emitting devices,[4] displays[5] and solar cells.[6] Conductive inkjet inks either contain conductive polymers,[7−9] carbon-based materials[10,11] or metal-based materials.[12−18] A high conductivity is usually desired and often crucial for the device performance, particularly for large-area devices. Metal-based inks offer unmatched performance in this regard; a resistivity of only 1.1−1.3 times the bulk metal has been achieved.[19] Silver nanoparticle (AgNP) ink is a common choice, due to a high conductivity and good stability in ambient conditions. However, the high cost of AgNP ink is problematic for cost-sensitive applications or large area coverage. Bulk Cu offers 95% of the electrical conductivity of Ag,[20] for a fraction of the cost. Therefore, CuNP ink formulations are potentially more cost-effective. However, the reactivity of CuNPs in ambient conditions makes ink development and postprocessing challenging compared to Ag. Li et al.[14] demonstrated reactive printing of Cu films on paper by the simultaneous printing of aqueous Cu-citrate solution and reducing agent, using thermal inkjet. Park et al.[15] synthesized CuNPs that were stable in solution, which they attributed to protection from oxidation by the polyvinylpyrrolidone (PVP) stabilizing agents. However, the sintering had to be performed in a vacuum to avoid oxidation. Efforts have been made to decrease reactivity by coating CuNPs with thin layers of less reactive materials, such as Ag[16] and C.[17] Nevertheless, oxidation remains an issue during oven-sintering in ambient conditions. Although low-temperature reduction and sintering has been shown with printed CuNP films, the resistivity has been at best 30−50 times larger than the bulk value.[14,17]

Roll-to-roll processes using low-cost plastic- or paper-based substrates require postprocessing that is quick and effective, as well as compatible with ambient conditions and temperature-sensitive substrates. Intense pulsed light processing (IPL) is a suitable method that briefly induces high film temperature by flash lamp exposure. Using a pulse duration of a few milliseconds or less, the heat transfer to the underlying substrate can be limited, avoiding damage. Thermal simulations estimated that a 300 μs flash pulse induces a film temperature exceeding 1000 °C, for a 1 μm thick silver film on top of a 150 μm thick substrate of polyethylene

Received: April 8, 2015
Accepted: August 6, 2015
Published: August 6, 2015

DOI: 10.1021/acsami.5b03061
ACS Appl. Mater. Interfaces 2015, 7, 18273−18282

terephthalate (PET).[21] According to the simulation, the PET substrate temperature never exceeds 250 °C, and falls below 150 °C within 8 ms. For CuNP films, IPL processing is particularly suitable, because oxide impurities can be effectively reduced due to the high peak temperature, if a reducing agent is present. Some commonly used ink solvents, such as ethanol and ethylene glycol can function as reducing agents, but to avoid reoxidation the pulse duration needs to be sufficiently short.[22] Dharmadasa et al.[22] used IPL processing with CuNP ink films, spray-coated on PET and glass. They observed that no reoxidation occurred with a pulse duration of 2 ms. The Cu_2O impurities of unsintered films were significant when using water as a solvent, but much less when using ethylene glycol. Ryu et al.[23] suggested that PVP will act as a reducing agent during IPL processing when used as a colloidal stabilizer for Cu/Cu_2O NPs. They proposed that PVP is decomposed by UV irradiation into an intermediate weak acid and/or hydroxyl end groups, acting like alcohol reductants. Araki et al.[24] developed different organic Cu-salt precursor inks that were screen printed on glass and processed with IPL. The Cu-salt precursor with the longest hydrocarbon chain length had the largest light absorption but still the highest resulting resistivity. The authors believed it was due to the evaporation of carbon that damaged the films, and to residual carbon remaining after sintering. Other interesting studies were performed by Hwang et al.,[25] who monitored the IPL sintering of a CuNP ink *in situ*; and Chung et al.,[26] who examined the IPL sintering of Cu precursor/CuNP hybrid inks.

One of the most promising methods of Cu film fabrication is the IPL processing of CuO NPs.[27,28] CuO NPs are less reactive in dispersion than the CuNP counterpart, and stable water-based inks have been made commercially available. Further, CuO NP inks can be acquired commercially at much lower cost (currently 75$/kg in bulk quantities[29]) than CuNP- or AgNP inks.

Inkjet printing technology is scalable to cover large areas and can be integrated into existing production environments at a comparably low cost. Inkjet is a noncontact method and therefore avoids contamination or damage to the substrates or previously deposited layers. Further, it is digital in its nature, which means that changes in the deposited patterns can be made quickly and easily. Inkjet requires a comparably low ink viscosity, the viable range for piezoelectric inkjet is approximately 5−30 mPa·s.[30] Low viscosity usually implies a low volume concentration of active material; therefore, a large amount of ink solvent needs to be quickly evaporated, or absorbed into the substrate. Quick evaporation from the substrate is possible by using volatile ink solvents and/or substrate heating. However, this also increases the evaporation rate at the nozzle−air interface, increasing the risk of inkjet nozzle clogging and therefore compromising the printing reliability. Furthermore, substrate heating is energy-consuming, and nontrivial to integrate in roll-to-roll environments. Utilizing absorption is an attractive alternative, in which paper substrates have inherent advantages. Besides the absorption capability, other advantages of paper are flexibility, low-cost and environmental sustainability. Inkjet-printed functional layers on paper typically require a high quality coating to reduce the surface roughness. With a suitable coating, the absorption rate can be increased as well, improving both pattern definition and functional performance.[31] Mesoporous coatings have been found particularly well suited for inkjet-printing of metal nanoparticle inks, because they provide a smooth surface combined with a high absorption rate.[32]

Paper substrates have previously been specially designed for the application in printed electronics.[33,34] Bollström et al.[33] developed a paper design with a thin smooth top coating. The authors paid special attention to precoatings with good barrier properties, to ensure suitability for organic semiconductor inks in various applications. However, paper substrates that facilitate IPL processing of NP-based inks have not been considered previously. In this study, we exploit a paper design using a mesoporous coating that is suitable for inkjet-printing of NP-based inks. Moreover, the paper design utilizes a novel, porous $CaCO_3$ precoating that increase the absorption and alters the surface chemistry. Recently, we showed that this paper design assisted low-temperature sintering of AgNP ink.[35] Here we demonstrate that the $CaCO_3$ precoating enhances reliability and effectiveness during IPL processing of CuO, thereby substantially improving the performance of inkjet-printed copper films.

2. EXPERIMENTAL SECTION

2.1. Manufacturing of Coated Paper Substrates. Two series of inkjet papers with mesoporous absorption coatings were manufactured. Each paper consisted of (i) base paper; (ii) precoating; (iii) absorption coating. Both series used the same base paper, and the same set of absorption coatings. The precoating differed between the series. One of the series used a traditional nonporous polyethylene (PE) precoating, referred to as the PE series. The other series used a porous $CaCO_3$ precoating, referred to as the $CaCO_3$ series. Each series consisted of 6 papers, where each paper had a different absorption coating pore radius. The different pore radii were derived from using boehmite alumina NP pigments with different crystallite size. The pigments used are referred to as HP8, HP10, HP14, HP16, HP18 and HP22, where the number indicates crystallite size in nanometers. For example, we will refer to the paper with PE precoating and HP10 coating as the HP10/PE paper. The base paper and the precoatings were manufactured and applied in industrial processes, whereas the absorption coatings were manually applied with a Meyer rod in the laboratory. The HP8/$CaCO_3$ paper had more coating surface defects than the others, and was therefore excluded from further use. The thicknesses of the layers in the finished papers were assessed with scanning electron microscopy (SEM) cross sections. Details of the inkjet papers have been given earlier[35] and are further described in this section. Three commercially available substrates were included for comparison; A PET film, a lightweight coated (LWC) paper and a mesoporous inkjet photopaper.

2.1.1. Base Paper. Eucalyptus cellular material was beaten as a 5% aqueous suspension (thick matter) using a refiner to a beating degree of 36° SR. The concentration of cellular material fibers in the thin matter was 1 wt %. Alkyl Ketene Dimer (AKD, 0.5 wt %) was added as internal sizing agent. Polyamine−polyamide−epichlorhydrin resin (Kymene, 0.4 wt %) was added as a wet-strength agent. Ground $CaCO_3$ (GCC, 10 wt %) was added as a filler. The quantities are given with respect to the fiber mass. The thin matter was transferred to the screen section of the paper machine and the web was dewatered, with further dewatering in press section and final drying with heated rollers. The obtained base paper was 190 μm thick, had a grammage of 160 g·m^{-2} and a moisture content of 7%.

2.1.2. PE Precoating. A resin formed of 100 wt % low density PE (LDPE, 0.92 g·cm^{-3}) was applied to the base paper in a laminator with melt extrusion lamination at a speed of 250 m·min^{-1}. The resulting PE layer thickness was approximately 20 μm.

2.1.3. $CaCO_3$ Precoating. Ground calcium carbonate (GCC, $CaCO_3$) with a $d_{50\%}$ of 0.7 μm, was mixed with styrene acrylate in 1:1 volume ratio. The mix was applied to the base paper with blade coating, resulting in an average thickness of approximately 20 μm.

2.1.4. Mesoporous Absorption Coatings. Coating dispersions were prepared, using boehmite alumina pigment powder ((AlO(OH), Sasol Disperal, 30 wt %) dispersed in water. The agglomerates were ground (IKA Ultra-Turrax) and electrostatically stabilized by addition of acetic acid (3 wt %). A small amount of chloride salt (KCl, 0.3 wt %) was added. PVA was used as a binder (Kuraray Mowiol 40-88), and boric acid as a hardener. The weight ratio of pigment:binder:hardener was 90:8:2. Six different dispersions were prepared, where only the pigment was varied. Each dispersion used a pigment with a specific crystallite size.

DOI: 10.1021/acsami.5b03061
ACS Appl. Mater. Interfaces 2015, 7, 18273−18282

The pigments used were from the Disperal series manufactured by Sasol, more specifically (in order of increasing crystallite size) Sasol Disperal HP8, HP10, HP14, HP16, HP18 and HP22. The numbers refer to the average crystallite size in nanometers. The average pigment particle diameter in the coating dispersions can be expected to be roughly 5 times the crystallite size according to the manufacturer. Each of the coating dispersions were applied on top of each precoating with a wire-bar applicator and dried in an oven for 15 min at 80 °C. This resulted in dry coating thicknesses of approximately 35 μm.

2.2. Substrate Characterization. Surface pH was measured with a flat membrane pH electrode (Mettler Toledo 403-34-S7/165), 20 min after deposition of a water film on top of the coating layer. Measurements were repeated 3 times at different spots. Pore radius characterization was performed using mercury porosimetry (Pascal 440 for the 3−50 nm range, Pascal 140 for the 50 nm to 100 μm range). Surface roughness was evaluated using atomic force microscopy (AFM, Nanosurf Easyscan2, tapping mode). Elemental composition analysis was made with energy dispersive X-ray spectroscopy (SEM-EDS, Jeol JSM-6610LV with Oxford INCA). Scanning electron microscopy (SEM) was performed with a Zeiss Merlin FEG-SEM and a Jeol JSM-6610LV.

2.3. Comparison Substrates. For comparison, the following three substrates were included in the study. (1) Nonporous PET film (Mitsubishi Hostaphan RN, 100 μm). Before printing, it was ultrasonicated in water for 15 min at 60 °C, rinsed in ethanol, distilled water, and dried. (2) Light-weight coated paper (LWC, SCA LWC GC80), having a thin coating consisting of $CaCO_3$/kaolin clay and styrene butadiene binder. (3) Commercial inkjet photopaper (HP Advanced Photo Paper), having a mesoporous alumina coating and a PE precoating.

2.4. Inkjet Printing. A commercially available, water-based CuO NP dispersion (Novacentrix ICI-002HV, 16 wt % CuO) was inkjet-printed. A piezoelectric inkjet printer (Dimatix 2831) was used to print horizontal conductors of nominal dimensions 20 × 0.4 mm between measurement pads. Ink cartridges with 10 pL drop volume were used (Dimatix 11610). For droplet actuation, a voltage of 20 V was used. The actuation waveform was supplied by the ink manufacturer. Drop spacing was set to 20 μm; nozzle- and platen temperatures were kept at a controlled room temperature of 22 °C.

2.5. IPL Processing. The CuO films were reduced and sintered simultaneously with IPL, using a machine developed in-house. The machine used a flash head with 7 in. reflector (Speedotron 102CC) and a high voltage xenon flash lamp (Speedotron MW8QVC). The pulse energy and pulse duration were set by changing the amount of capacitance (50−2400 μF, 47 steps), the capacitor bank voltage (500−1500 V, variable), and the pulse-forming inductor (0−1 mH, 6 steps). An inductor of L = 1 mH (DCR = 9 mΩ) was used throughout these experiments. A simplified schematic is shown in the Supporting Information, Figure S1a. Pulse waveforms were captured using a photodiode circuit, connected to an oscilloscope. Pulse durations were determined according to t_{10}, the time during which the intensity is above 10% of maximum intensity. The exposure energy E (J·cm^{-2}) was estimated as follows. We assume that 50% of the discharged electrical energy is converted to light energy (usual approximation of the efficiency of high power xenon flash tubes), and that the discharged electrical energy equals the capacitor bank energy, neglecting resistive losses. Further, we assume a uniform distribution of light within the reflector output area, so that we have $E = C \cdot U^2/(\pi \cdot d)$ where C is the capacitance in F, U is the bank voltage in V and d is the reflector diameter in cm. The samples were predried in an oven at 60 °C and then placed 3 cm from the reflector edge (Supporting Information, Figure S1b). A range of pulse conditions was examined for each substrate (pulse setting and number of pulses). The aim was to achieve the lowest resistivity, while avoiding delamination and reoxidation of the Cu film. The pulse settings that were found most effective are shown in detail in the Supporting Information, Table S1. The corresponding pulse waveforms are shown in the Supporting Information, Figure S2.

2.6. X-ray Diffraction. X-ray diffraction was performed on powders from CuO ink and IPL-processed Cu films, using a diffractometer (Bruker D2 Phaser), equipped with a monochromatic Cu Kα radiation source. The characterization was made in θ−θ geometry, using a low-background Si single crystal sample holder (Bruker). The CuO powder was prepared by applying the CuO ink to a standard microscope glass slide, letting it dry at 90 °C for a few hours, and scraping it off. The Cu powder samples were prepared by IPL-processing of CuO films on the papers HP14/PE and HP14/$CaCO_3$. The IPL exposure was 3 pulses, each with 1.85 J·cm^{-2} (2.3 ms). After processing, Cu powder was carefully scraped off. Overview data was collected using a 0.6 mm entrance slit (steps of 0.05°, 0.5 s/step), whereas higher-resolution data of the first diffraction peaks was collected using a 0.1 mm entrance slit (steps of 0.02°, 3 s/step).

2.7. Resistance Measurements and Resistivity Calculations. Conductor resistance was measured with 4-point probes, using a source-meter in current source mode (Keithley 2611A). Averages and standard deviations of resistivity are based on resistance measurements of 8 conductors for each substrate. The resistivity is calculated from the measured resistance by using the relation $R = \rho \cdot L \cdot (w \cdot h)^{-1}$ where ρ is the resistivity, R is the resistance and w, h and L are the conductor width, height and length, respectively. The height of the Cu conductors was determined after IPL processing to h = 0.32−0.50 μm (AFM, Nanosurf Easyscan2). The width and length were determined to w = 430 μm and L = 20 mm (microscope camera, Dimatix).

3. RESULTS AND DISCUSSION

Figure 1a shows a TEM image of CuO NPs from the water-based inkjet dispersion. The NPs have varying form and a wide size

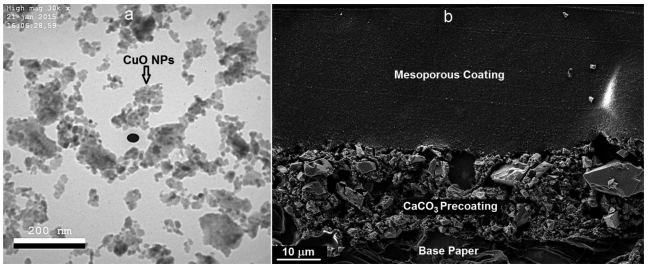

Figure 1. (a) TEM image of CuO NPs from the inkjet dispersion. Note the broad size distribution. (b) SEM image of a cross section of a paper with porous $CaCO_3$ precoating. Some of the large $CaCO_3$ pigments have been detached during the mechanical sectioning. Note that only the upper part of the base paper is shown.

distribution of approximately 10−300 nm. Figure 1b shows a SEM cross section of the custom-designed inkjet paper with a mesoporous absorption coating and a porous $CaCO_3$ precoating.

3.1. Characterization of Absorption Coatings. *3.1.1. Surface Morphology.* The range of characteristic pore radius was 9−32 nm for the PE series and 16−38 nm for the $CaCO_3$ series (Table 1). We have defined the characteristic pore radius as the

Table 1. Characteristic Pore Radius of the Different Mesoporous Coatings on top of a PE Precoating and a $CaCO_3$ Precoating[a]

	HP8	HP10	HP14	HP16	HP18	HP22
PE	9	13	18	22	25	32
$CaCO_3$		16	22	28	32	38

[a]Values in nanometers.

maximum of the pore radius distribution, as given by mercury porosimetry. By this definition, the characteristic pore radius represents the pores with the largest contribution to the total pore volume of the coating.

The $CaCO_3$ series had a slightly larger pore radius for a given pigment size. This is likely due to an increased tendency of pigment flocculation during the coating application, as well as the

DOI: 10.1021/acsami.5b03061
ACS Appl. Mater. Interfaces 2015, 7, 18273−18282

larger surface roughness of the $CaCO_3$ precoating, possibly affecting the packing of the coating pigments. RMS surface roughness (Sq) over 20 × 20 μm was 24−39 nm, measured on the HP10 and HP22 absorption coatings on both types of precoatings. It is expected that all papers have Sq values within this range, because the papers that were not measured, have intermediate pigment sizes and characteristic pore radii. Surface roughness on the comparison LWC paper was the highest, with Sq = 56 nm. The PET film had the lowest roughness, with Sq = 7 nm. The morphology characterization indicated that all substrates in this study were sufficiently smooth to allow a continuous film formation.

3.1.2. Surface Chemistry. Surface composition analysis revealed that the surface on papers with $CaCO_3$ precoating contained measurable amounts of Cl and Ca. With quantitative EDS, the concentrations were estimated to 0.3−0.5 wt % of Cl and approximately 0.4 wt % of Ca. The surface of papers with PE precoating contained no Ca, and the concentration of Cl was below the limit of quantification. We have previously observed that the small presence of Cl with this paper design induced coalescence of Ag NPs.[35] Therefore, we used SEM imaging of the unprocessed CuO films to examine any possible aggregation of CuO NPs for each paper series. No difference in CuO layer morphology was noted with the different precoatings (Supporting Information, Figure S3). Surface pH measurements showed that the mesoporous coatings on the PE precoated series were acidic with surface pH 4.3−4.8, whereas the $CaCO_3$ precoating rendered the coatings alkaline with pH 7.1−8.3 (Table 2). Evidently, the $CaCO_3$ precoating has an active effect on the surface chemistry, with respect to elemental composition and pH value.

Table 2. Average Surface pH on Each Mesoporous Coating Combined with Each Type of Precoating[a]

	HP8	HP10	HP14	HP16	HP18	HP22
PE	4.6	4.8	4.8	4.5	4.4	4.3
$CaCO_3$		7.1	7.4	7.5	7.9	8.3

[a]Coatings on top of the PE precoating are naturally acidic, whereas the $CaCO_3$ precoating renders the coatings alkaline. The average standard deviation is ±0.10.

3.2. IPL Processing of CuO Patterns. To compare IPL processing results between papers, a pulse condition of 3 pulses, each with $E = 2.7$ J·cm^{-2} and $t = 2.9$ ms was used (3 × 2.7 J·cm^{-2}). This was chosen as a suitable setting for comparison, because it occasionally damaged films on a few papers but did not damage films on most papers. Figure 2a shows the resistivity of IPL-processed, inkjet-printed Cu films versus the characteristic pore radius of the coatings. Using the paper series with PE precoating, the resistivity was at best 4.7 ± 0.45 $\mu\Omega$·cm. There were delamination issues, particularly with two of the papers (HP8/PE and HP22/PE). With the HP8 coating (which has the smallest pigments), delamination was more frequent and more severe than with the rougher coatings (HP10-HP18). It is possible that the smoother surface of HP8/PE decreases the layer adhesion, as predicted by the mechanical theory of fundamental adhesion.[36] IPL processing with 3 × 2.7 J·cm^{-2} resulted in infinite resistivity on the HP22/PE paper. This was because the films suffered from cracks to a greater extent than on the other coatings, rendering them nonconductive. The cracks coincided with coating defects, which were larger on HP22/PE than for the other papers. Apparently, coating defects increase the risk of film cracks during IPL processing. Using the paper series with $CaCO_3$ precoating, the CuO films were effortlessly processed into highly conductive Cu for the entire series. The conductivity exceeded 40% of the bulk metal conductivity with all coatings. The best performance resulted on the HP14/$CaCO_3$ paper, with a resistivity of 3.4 ± 0.25 $\mu\Omega$·cm. Film delamination did not occur on any paper in the $CaCO_3$ series, and the resistivity was not much affected by coating pore radius variations in the 16−38 nm range.

3.3. Optimization of IPL Conditions. The IPL exposure of 3 × 2.7 J·cm^{-2} was not reliable on the papers with PE precoating, because it occasionally damaged or delaminated part of the films. Therefore, further optimization of pulse conditions was performed to compare the precoatings. The HP14 paper from each series was selected because it showed the best and most consistent results.

3.3.1. PE Precoating. With the HP14/PE paper, a reduction in pulse energy to 1.5 J·cm^{-2} ($t = 2.3$ ms) was appropriate to remove

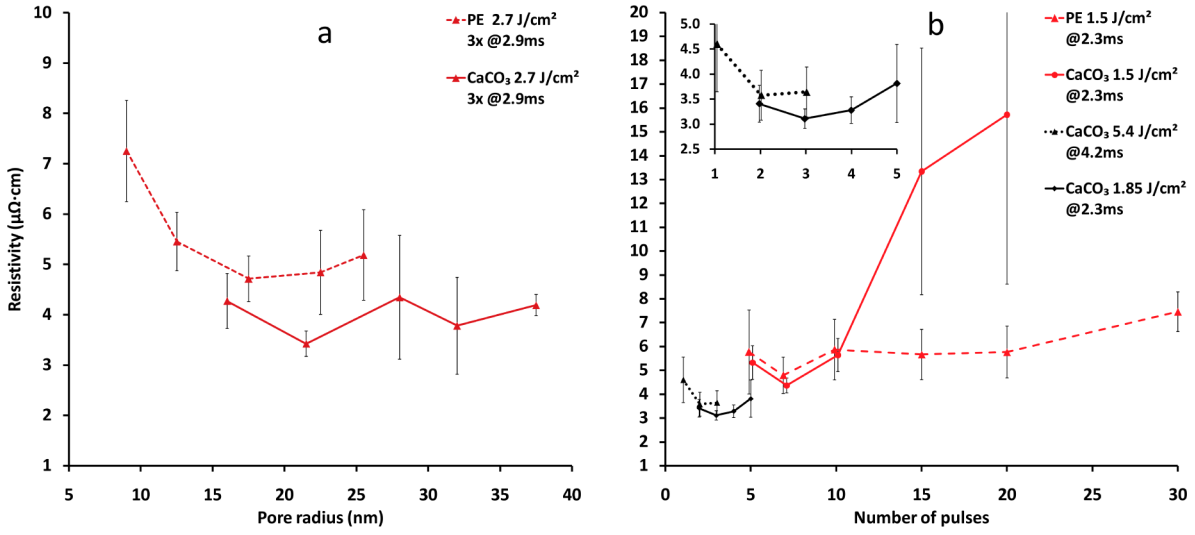

Figure 2. Resistivity of IPL processed, inkjet-printed Cu films on paper. (a) Versus characteristic pore radius. The $CaCO_3$ precoating reduced the resistivity. (b) Versus number of IPL pulses (HP14 coating). The black curves represent reliable conditions with the $CaCO_3$ precoating. The red dashed curve represents the best reliable conditions with the PE precoating. Note that the $CaCO_3$ precoating allowed effective IPL processing using a single pulse. The inset shows the bottom left region magnified. The error bars correspond to ±1 standard deviation.

DOI: 10.1021/acsami.5b03061
ACS Appl. Mater. Interfaces 2015, 7, 18273−18282

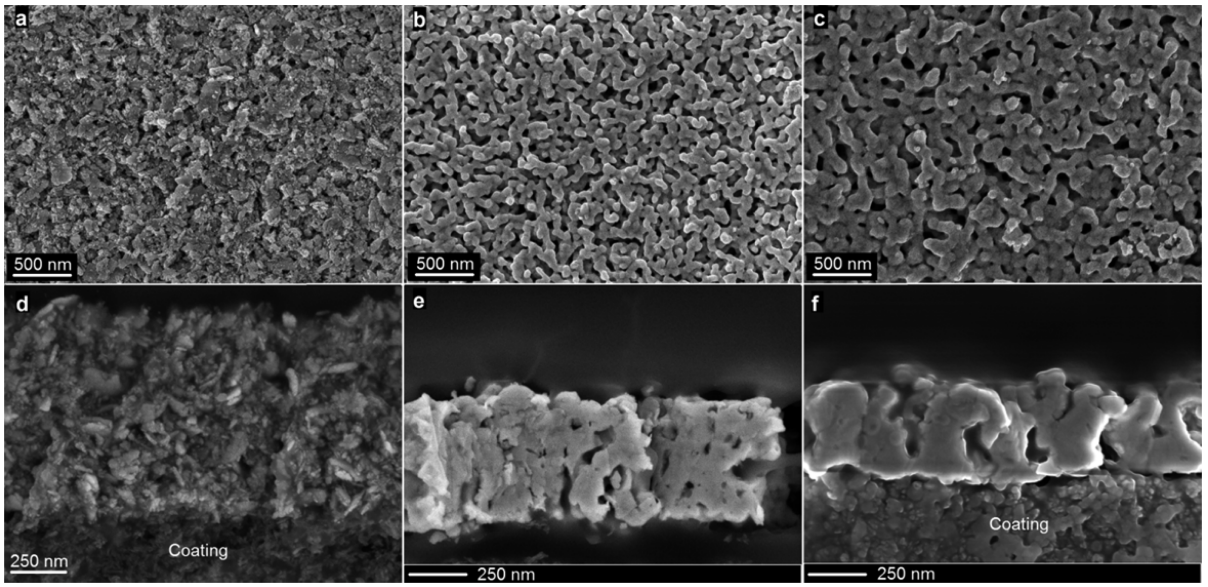

Figure 3. SEM images of inkjet-printed CuO film on paper, before and after IPL processing using 3×1.85 J·cm^{-2} and HP14 coating. Top of films shown in (a–c) and corresponding cross sections shown in (d–f). Using the $CaCO_3$ precoating enhances the effect of the processing, resulting in increased microstructure size, higher density and higher conductivity. (a,d) Unprocessed CuO. (b,e) IPL-processed Cu (PE precoating). Note that the film has delaminated from the coating. (c,f) IPL-processed Cu ($CaCO_3$ precoating).

all delamination tendencies. Figure 2b shows the resistivity of Cu films versus the number of IPL pulses. At 1.5 J·cm^{-2}, at least 5 pulses were required to reduce the CuO film into conductive Cu, resulting in a resistivity of 5.7 ± 1.7 $\mu\Omega$·cm. Using 7 pulses was most effective, minimizing the resistivity to 4.7 ± 0.8 $\mu\Omega$·cm. Using more than 7 pulses, the resistivity increased, although it remained low and fairly constant until above 20 pulses, when cracks in the films appeared and increased the resistivity further (Figure 2b, dashed). No reoxidation was noticed on the HP14/PE paper.

3.3.2. $CaCO_3$ Precoating. Also, at the fairly low pulse energy of 1.5 J·cm^{-2} (2.3 ms), the $CaCO_3$ precoating lowered the film resistivity and its variations. Similar to the PE variant, the reduction threshold on HP14/$CaCO_3$ was 5 pulses at 1.5 J·cm^{-2}, and the minimum resistivity (4.4 ± 0.7 $\mu\Omega$·cm) was reached with 7 pulses. However, using 10 pulses or more, the films started to reoxidize, greatly increasing average resistivity and resistivity variations (Figure 2b, red, solid). With the $CaCO_3$ precoating, pulse energies could be reliably increased, reducing resistivity further. All tested pulse settings, including the maximum output capability of 5.4 J·cm^{-2} (4.2 ms), were usable without delamination. The most effective pulse condition was 2–4 pulses of 1.85 J·cm^{-2} (2.3 ms), allowing consistent results around 3.4 $\mu\Omega$·cm (Figure 2b, black, solid). Minimum resistivity was achieved using 3 pulses of 1.85 J·cm^{-2} (2.3 ms), resulting in a resistivity as low as 3.1 ± 0.2 $\mu\Omega$·cm. This corresponds to more than half of the conductivity of bulk copper, which is higher than has been previously reported for IPL-processed Cu films. Figure 3 shows SEM images of inkjet-printed CuO films, before and after IPL processing using both type of precoatings. The cross section in Figure 3d shows that the CuO film did not mix into the coating, because the coating pore size was sufficiently small to prevent CuO NP intrusion. The broad CuO NP size distribution of approximately 10–300 nm is arguably beneficial for the dense packing of the CuO NP film. Note that the IPL conversion to Cu increased the material density and reduced the film thickness significantly. The largest densification resulted with the $CaCO_3$ precoating (Figure 3f). Thus, for equal IPL exposure, using the $CaCO_3$ precoating resulted in increased microstructure size, higher density and higher conductivity.

A complete predrying of the substrate was observed to be beneficial for the IPL process. If the IPL exposure vaporizes any remaining water or additives, the induced pressure gradient may damage or delaminate the film. We observed that the $CaCO_3$ precoating significantly reduced the need for predrying. Therefore, we postulate that the main factor explaining the enhanced IPL processing using the $CaCO_3$ precoating is the high porosity of the precoating, allowing water and ink additives to quickly pass through it. In contrast, the PE precoating acts as a barrier, keeping water and additives directly underneath the CuO film. Note that even with a complete predrying, nonporous substrates or barriers trap nonvolatile ink additives within or below the film, likely damaging the film during the IPL process.

3.4. X-ray Diffraction. Figure 4 shows X-ray diffraction patterns for dried CuO ink, IPL-processed Cu on PE-precoated paper and IPL-processed Cu on $CaCO_3$-precoated paper. The overview scans show that the patterns are dominated by the phases CuO and Cu, respectively. The diffuse background increasing toward the low-angle side is due to the Si sample holder. The first diffraction peak in CuO is rather broad. If we assume a shape factor of 0.9, and that all line broadening is due to a finite size of the crystallites, the Scherrer equation estimates the average crystallite size to approximately 12 nm. This is comparable with the smallest CuO NPs that was observed using TEM imaging, indicating a reasonable estimate. The first diffraction peak from the Cu, processed on PE-precoated paper, is significantly sharper. Crystallite size estimation using the Scherrer equation yields an average of approximately 28 nm. The Cu processed on $CaCO_3$-precoated paper shows a yet sharper peak, indicating an average crystallite size of 36 nm. This is consistent with the SEM images, indicating that the $CaCO_3$ precoating favors a more effective IPL material conversion.

3.5. IPL Processing Results on the Comparison Substrates. Figure 5 shows microscope images of films on various substrates, after different IPL processing conditions.

DOI: 10.1021/acsami.5b03061
ACS Appl. Mater. Interfaces 2015, 7, 18273–18282

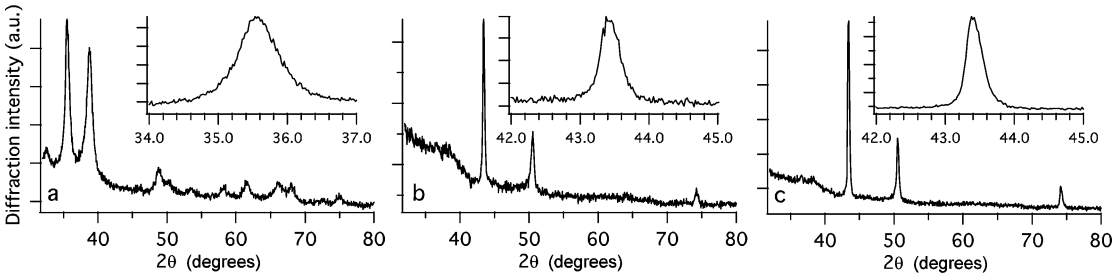

Figure 4. X-ray diffraction patterns. (a) Dried CuO ink. (b) IPL-processed Cu on paper (PE precoating). (c) IPL-processed Cu on paper ($CaCO_3$ precoating). The insets show the first diffraction peak in magnification. IPL processing using 3 × 1.85 J·cm^{-2} (HP14 coating).

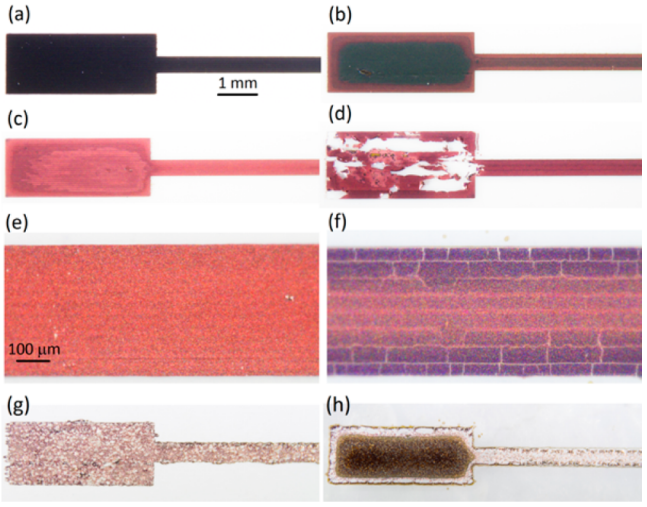

Figure 5. Microscope images of films on custom papers with HP14 coating (a–f) and comparison substrates (g–h). (a) Unprocessed CuO. (b) PE, 4 × 1.5 J·cm^{-2}, insufficient energy, pad interior not reduced. (c) $CaCO_3$, 3 × 2.7 J·cm^{-2}, fully reduced without delamination. (d) PE, 3 × 2.7 J·cm^{-2}, delamination. (e) $CaCO_3$, 3 × 5.4 J·cm^{-2}, no reoxidation (thin section magnified). (f) $CaCO_3$, 5 × 5.4 J·cm^{-2}, reoxidation and cracks (thin section magnified). (g) LWC paper, 1 × 5.4 J·cm^{-2}, fully reduced but severely damaged by delamination. (h) PET substrate, 3 × 2.7 J·cm^{-2}, no conductivity.

With the PET film, exposure conditions allowing conductive Cu films were not found. At energy levels sufficiently high for reduction, the film was severely damaged (Figure 5h). With the LWC paper, conductive films resulted, although largely affected by delamination. The most successful exposure condition was a single pulse with 5.4 J·cm^{-2}. This reduced the film effectively, but inflicted spot-wise delamination (Figure 5g). With pulse energies sufficiently low to avoid delamination, the CuO films could not be reduced. The commercial inkjet photopaper allowed successful processing without delamination with careful energy tuning, but processing of larger-area patterns was challenging due to local delamination. The results were similar to results with the PE-precoated custom papers. This is not surprising, because the photopaper has a similar construction using a mesoporous alumina absorption coating and a PE precoating. Various studies of solution-processed Cu film deposition have been previously published, using different combinations of deposition methods, inks, substrates and processing methods. Table 3 shows an overview comparison with this study.

3.6. Important Issues Limiting Reliability. We identified the most notable issues during the IPL process to be delamination, reoxidation, adhesion loss and crack formation. These issues all limited the reliability and performance of the resulting Cu films. Each issue is described in the following sections.

3.6.1. Delamination. Delamination and other film damage occurred on papers with PE precoating. The problem increased with higher exposure energy but could be minimized by using multiple pulses at 1.5 J·cm^{-2}. The range of usable pulse energies was narrow, and the IPL processing reliability was therefore compromised. Further challenges emerge from a feature size influence on delamination, and necessary reduction energy. At smaller features and edges, the reduction occurred at lower energy, while interior parts and larger features required higher energy (Figure 5b). However, when increasing the energy, delamination commonly occurred at such interiors and larger features (Figure 5d). Feature-size dependence has been observed earlier by Paquet et al.,[28] who used IPL processing of inkjet-printed CuO NPs on coated PET substrates. They concluded that the result was dependent on the feature size in the pattern, and suggested that the ink reduction agent diffuses in the coating to a larger extent if the feature size is large. In this study, the $CaCO_3$ precoating substantially expanded the usable energy range and improved the IPL processing reliability and performance (Figure 5c). The main reason for this is likely that the porosity of the $CaCO_3$ precoating allowed ink solvents and additives to be removed from the immediate vicinity of the CuO film, and therefore prevented IPL-induced evaporation of such ink components to inflict delamination and other film damage.

3.6.2. Reoxidation. With the $CaCO_3$ precoating, the films reoxidized when subject to excessive multipulse exposure (Figure 5f). There was no visible reoxidation with the PE precoating. This is arguably due to the addition of acetic acid in the coating dispersions. It is known that the presence of acetic acid helps reduction of CuO.[39] However, when applied to the $CaCO_3$ precoating, acetic acid is consumed to form calcium acetate according to $CaCO_3 + 2CH_3COOH \rightarrow Ca(CH_3COO)_2 + CO_2 + H_2O$. Therefore, the Cu reoxidation that was observed on the $CaCO_3$ series, is likely due to the loss of acetic acid and its reducing effect. Because of the loss of a potential reduction agent, one could expect the $CaCO_3$ precoating to be unfavorable for the IPL reduction reaction. However, no distinct difference was noted in the energy threshold for reduction, which was around 5 × 1.5 J·cm^{-2}, for both precoating types.

3.6.3. Loss of Adhesion. Figure 6 shows adhesion comparisons before and after IPL processing, using PE precoating or $CaCO_3$ precoating. For both paper series, the adhesion of the CuO films before IPL processing was strong, and tape tests only removed a top layer from the CuO films (Figure 6a,d). However, the IPL processing impaired the adhesion considerably. Tape tests completely removed the Cu film on the PE-precoated paper (Figure 6b), and almost completely removed the Cu film on the $CaCO_3$-precoated paper (Figure 6e). Additional adhesion comparisons of processed Cu films was made by cutting cross-hatch patterns in the films with a scalpel (approximately 1 mm spacing between cuts). On the PE precoated paper, the film

DOI: 10.1021/acsami.5b03061
ACS Appl. Mater. Interfaces 2015, 7, 18273–18282

Table 3. Overview of Studies Demonstrating Solution-Processed Cu Films

ink material	deposition	substrate	sintering	resistivity [$\mu\Omega$·cm]	ref
CuNP/PVP	inkjet	polyimide	oven 200 °C/1 h	3.6	13
Cu-salt+reducer	inkjet	paper	room temperature	55	14
CuNP/PVP	inkjet	glass	oven 325 °C/1 h (VAC)	17.2	15
CuNP/AgNP	inkjet	glass	oven 300 °C (N_2)	11	16
CuNP/graphene	inkjet	polymer	room temperature	100	17
CuNP	spraycoating	PET/glass	IPL	96	22
CuNP/Cu_2O	inkjet	polyimide	IPL	5	23
Cu-salt	screen	glass	IPL	56	24
CuO NP[a]	inkjet	coated PET	IPL	5.5	27
CuO NP[a]	inkjet	coated PET	IPL	9	28
CuNP	drop dispensing	PET	IPL	5	37
CuNP/CuMP			IPL	80	38
CuO NP[a]	inkjet	coated paper	IPL	3.1	this study

[a]Novacentrix Metalon ICI-002HV.

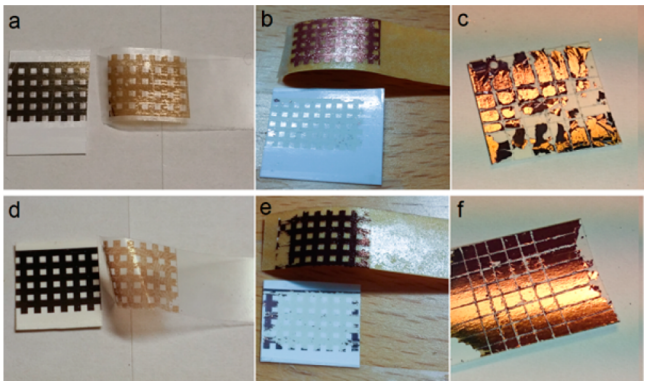

Figure 6. Adhesion tests on papers with HP14 coating, before and after IPL processing with 3 × 1.85 J·cm^{-2}. Tests on PE precoated paper shown in (a–c) and tests with $CaCO_3$ precoated paper shown in (d–f). Adhesion loss was problematic during IPL processing, but the $CaCO_3$ precoating showed an improvement. (a) PE, tape test of unprocessed CuO. (b) PE, tape test after IPL. (c) PE, cross-cut test after IPL. (d) $CaCO_3$, tape test of unprocessed CuO. (e) $CaCO_3$, tape test after IPL. (f) $CaCO_3$, cross-cut test after IPL.

delaminated severely near the cuts due to weak adhesion (Figure 6c). However, on the $CaCO_3$ precoated paper, the delamination was less severe (Figure 6f). Conclusively, adhesion loss during the IPL processing was reduced using the $CaCO_3$ precoating. Nevertheless, adhesion loss during IPL processing remains a problem. Post-treatment such as lamination or lacquering could be an alternative to reduce issues with weak adhesion, and should protect against reoxidation as well.

3.6.4. Crack Formation. Small cracks in the film sometimes occurred, usually with the cracks coincident with film irregularities. Film irregularities were typically due to either coating defects or to the printing process. Only a few inkjet nozzles were active, thus the films were printed using several passes. Each pass requires a few seconds, allowing the adjacent part of the film to partially dry. Therefore, ridge-like irregularities were created by the printing process that tended to initiate cracks during the IPL processing (Supporting Information, Figure S4). This is consistent with previous observations by Kang et al.,[27] who noted crack formation along the printing direction. Film irregularities can be seen as local thickness gradients, likely inflicting local thermal stress during IPL exposure. This probably initiates the crack formation. Repeated pulses of already converted Cu films increased the risk of cracks. We expect that the occurrence of cracks can be decreased by (1) Using an industrial coating and drying process for the top coatings, to minimize coating defects. (2) Printing the films/patterns with a system allowing high uniformity of thickness. For an inkjet system in particular, the nozzle array should be wide enough to print each pattern in a single pass. By minimizing the risk of film cracks, the performance and reliability of the films should be further improved.

3.7. IPL Processing of Patterns with Larger Area. IPL processing is particularly challenging for patterns with larger area and varying feature size, because the optimal exposure tends to be dependent on feature size. In addition, the intensity will not be perfectly uniform across the exposure area, thus larger patterns are less likely to be evenly exposed. Figure 7b–e shows IPL processing results of 5 × 5 cm, or larger, areas. Using the PE precoating, or the commercial photopaper, the processing was difficult. Some parts of the patterns could not be fully reduced without damaging other parts. However, with the $CaCO_3$ precoating, the patterns were much more reliably processed. The inset of Figure 7b shows in magnification that features of different size are uniformly processed and free from damage.

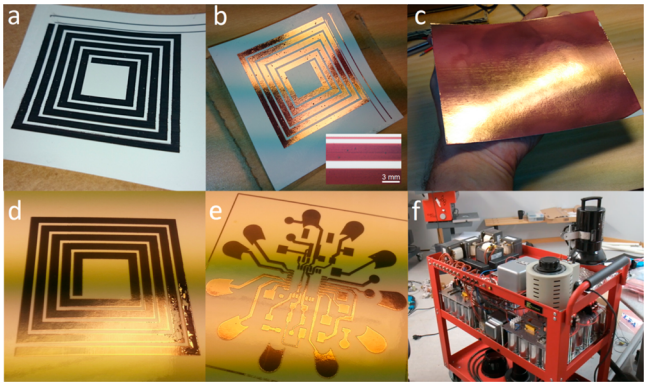

Figure 7. Inkjet-printed patterns and rod-coated film, for IPL-processing on custom-designed paper (HP14/$CaCO_3$). The size of the printed patterns is approximately 5 × 5 cm. (a) Unprocessed antenna (inkjet-printed CuO). (b) Antenna after IPL processing. Inset shows magnified part. (c) Rod-coated large-area film after IPL-processing. (d) Antenna pattern on commercial photopaper. Note the nonuniform IPL conversion and local delamination. (e) Circuit board. (f) Custom-built IPL processing machine.

DOI: 10.1021/acsami.5b03061
ACS Appl. Mater. Interfaces 2015, 7, 18273–18282

4. SUMMARIZING DISCUSSION

Mesoporous coated papers are well suited for inkjet printing, due to a comparably low surface roughness and a fast liquid absorption. Here, we have found them to also have attractive properties for IPL processing. The bright coatings have high reflectance and temperature stability, as well as low thermal conductivity due to high porosity. In contrast, the dark CuO film will absorb wide-band pulsed light effectively. However, when using IPL energy sufficiently high to completely reduce the CuO film, the challenge remains to avoid delamination and other film deformation. The expanded range of effective pulse conditions that was enabled by the $CaCO_3$ precoating is important, because it substantially improved the processing reliability and performance, particularly when the patterns consisted of varying line widths and feature sizes. Further, the possibility to increase pulse energy and decrease the number of pulses, allows reducing the total IPL energy consumption.

We have previously concluded that effective sintering greatly reduces the importance of ink-substrate interactions.[32,35] IPL processing is a special case, because the sintering itself depends on suitable ink-substrate interactions for its effectiveness. In addition to chemical and mechanical interactions that we have discussed here and earlier,[32,35] we need to include the conceptions of optical- and thermal interactions to improve the understanding of the IPL process. Optical interaction can be exemplified by the total light absorption of the film and its dependence on substrate properties such as roughness and internal scattering. Tobjörk et al.[40] used continuous IR-radiation to sinter inkjet-printed AgNPs and AuNPs on paper. The light absorption of those films were larger on paper than on a plastic or glass substrate. This was explained mainly by the multiscattering properties of the papers. They also observed less problems with cracks in the films on paper, compared to a plastic or glass substrate.

Thermal interaction involves the thicknesses, geometry, and thermal properties of the film and substrate, as well as the interface heat transfer properties. A low thermal conductivity of the substrate, will imply a higher film temperature. In the systems involved here, the material compositions are heterogeneous and the temperature swings are large. Assessing the effective thermal properties and how they change during the process is not trivial. However, we can safely assume that the base paper, precoatings and coatings used here, all have low thermal conductivity. Solid low-density PE has a thermal conductivity of 0.3 $W{\cdot}m^{-1}{\cdot}K^{-1}$. Gane et al.[41] determined conductivity of $CaCO_3$ pigments with latex binders to 0.08−0.13 $W{\cdot}m^{-1}{\cdot}K^{-1}$. The mesoporous boehmite alumina coatings have low thermal conductivity due to a very high porosity.[42] Ideally, the thermal expansion should be similar for the layers; the film-coating interface is obviously the most important. With a large thermal expansion mismatch, the risk of film cracks will increase. The $CaCO_3$ precoating improved the thermal- and dimensional stability of the papers compared with the PE precoating, which was confirmed by oven-heating papers at 180 °C. The enhanced thermal stability of the $CaCO_3$ precoated papers is possibly a contributing factor to the observed advantages during IPL processing. Further, the $CaCO_3$ precoating had an impact on the paper surface chemistry, which potentially affects the CuO film reduction during the IPL exposure. However, there was no notable change in the lowest required IPL energy for reduction, and the tendency for reoxidation during the IPL exposure increased. Neither did the altered surface chemistry notably affect the CuO NP film morphology. Therefore, the advantages for IPL processing that was evident with this paper design, should be attributed mainly to the large absorption capability conveyed by the $CaCO_3$ precoating.

Note that chemical, physical, optical and thermal properties of the film will undergo radical changes during the IPL material conversion. As the dark CuO NP film is converted into a reflective Cu film, the light absorption decreases and the thermal conductivity increases, limiting heating rate and peak temperature. This may be seen as a negative feedback mechanism, stabilizing the process and reducing the risk of thermal runaway. Still, IPL processing requires a carefully tailored combination of ink, substrate and process conditions to achieve high performance conductive films.

5. CONCLUSION

Inkjet fabrication of highly conductive copper patterns was performed by utilizing coated papers of a special design. The fabrication was conducted in ambient conditions using intense pulsed light processing (IPL) of a water-based CuO dispersion. The effectiveness and reliability of the IPL processing were improved by using papers with a porous $CaCO_3$ precoating beneath the absorption layer. The performance advantage remained over a range of coating pore sizes, as well as when compared with several types of commercial substrates. A resistivity of 3.08 ± 0.15 $\mu\Omega{\cdot}cm$ was achieved, corresponding to more than 50% of the conductivity of bulk copper.

IPL processing of CuO patterns with varying feature size is often challenging, because the suitable exposure energy tends to be dependent on feature size. Importantly, the $CaCO_3$ precoating increased the viable range of exposure energy, and therefore improved the processing reliability. The beneficial effect of the $CaCO_3$ precoating can arguably be attributed mainly to its porosity, allowing effective removal of the water and ink additives. This reduces the risk of film damage and delamination during the IPL exposure.

■ ASSOCIATED CONTENT

Supporting Information

The Supporting Information is available free of charge on the ACS Publications website at DOI: 10.1021/acsami.5b03061.

Principle schematic of IPL circuit, image of sample placement, table of IPL pulse settings, graph of pulse waveforms, SEM images of crack formation, SEM images of CuO film morphology (PDF).

■ AUTHOR INFORMATION

Corresponding Author

*T. Öhlund. E-mail: thomas.ohlund@gmail.com.

Notes

The authors declare no competing financial interest.

■ ACKNOWLEDGMENTS

We gratefully acknowledge financial support from the Knowledge Foundation, the Swedish Agency for Economic and Regional Growth and the European Regional Development Fund. The funding sources had no involvement in this article. We acknowledge Dr. Wolfgang Schmidt and the Felix Schoeller Group, Osnabruck, Germany for important contributions in the design and manufacturing of the papers. For SEM imaging, we acknowledge Dr. Nikki Lee and the Umeå Core Facility for

DOI: 10.1021/acsami.5b03061
ACS Appl. Mater. Interfaces 2015, 7, 18273−18282

Electron Microscopy (UCEM) at Umeå University. We thank Prof. Magnus Norgren for valuable discussions.

REFERENCES

(1) Sridhar, A.; van Dijk, D. J.; Akkerman, R. Inkjet Printing and Adhesion Characterisation of Conductive Tracks on a Commercial Printed Circuit Board Material. *Thin Solid Films* **2009**, *517*, 4633−4637.

(2) Shaker, G.; Safavi-Naeini, S.; Sangary, N.; Tentzeris, M. M. Inkjet Printing of Ultrawideband (UWB) Antennas on Paper-Based Substrates. *Antenn. Wireless Propag. Lett., IEEE* **2011**, *10*, 111−114.

(3) Liana, D. D.; Raguse, B.; Gooding, J. J.; Chow, E. Recent Advances in Paper-Based Sensors. *Sensors* **2012**, *12*, 11505−11526.

(4) Sandström, A.; Dam, H. F.; Krebs, F. C.; Edman, L. Ambient Fabrication of Flexible and Large-Area Organic Light-Emitting Devices Using Slot-Die Coating. *Nat. Commun.* **2012**, *3*, 1002.

(5) Kang, H.; Jung, S.; Jeong, S.; Kim, G.; Lee, K. Polymer-Metal Hybrid Transparent Electrodes for Flexible Electronics. *Nat. Commun.* **2015**, *6*, 6503.

(6) Lee, J.-Y.; Connor, S. T.; Cui, Y.; Peumans, P. Solution-Processed Metal Nanowire Mesh Transparent Electrodes. *Nano Lett.* **2008**, *8*, 689−692.

(7) Yoon, H.; Jang, J. Conducting-Polymer Nanomaterials for High-Performance Sensor Applications: Issues and Challenges. *Adv. Funct. Mater.* **2009**, *19*, 1567−1576.

(8) Yoshioka, Y.; Jabbour, G. E. Desktop Inkjet Printer as a Tool to Print Conducting Polymers. *Synth. Met.* **2006**, *156*, 779−783.

(9) Sirringhaus, H.; Kawase, T.; Friend, R. H.; Shimoda, T.; Inbasekaran, M.; Wu, W.; Woo, E. P. High-Resolution Inkjet Printing of All-Polymer Transistor Circuits. *Science* **2000**, *290*, 2123−2126.

(10) Kordás, K.; Mustonen, T.; Tóth, G.; Jantunen, H.; Lajunen, M.; Soldano, C.; Talapatra, S.; Kar, S.; Vajtai, R.; Ajayan, P. M. Inkjet Printing of Electrically Conductive Patterns of Carbon Nanotubes. *Small* **2006**, *2*, 1021−1025.

(11) Huang, L.; Huang, Y.; Liang, J.; Wan, X.; Chen, Y. Graphene-Based Conducting Inks for Direct Inkjet Printing of Flexible Conductive Patterns and their Applications in Electric Circuits and Chemical Sensors. *Nano Res.* **2011**, *4*, 675−684.

(12) Li, Y.; Wu, Y.; Ong, B. S. Facile Synthesis of Silver Nanoparticles Useful for Fabrication of High-Conductivity Elements for Printed Electronics. *J. Am. Chem. Soc.* **2005**, *127*, 3266−3267.

(13) Lee, Y.; Choi, J.-r.; Lee, K. J.; Stott, N. E.; Kim, D. Large-Scale Synthesis of Copper Nanoparticles by Chemically Controlled Reduction for Applications of Inkjet-Printed Electronics. *Nanotechnology* **2008**, *19*, 415604.

(14) Li, D.; Sutton, D.; Burgess, A.; Graham, D.; Calvert, P. D. Conductive Copper and Nickel Lines via Reactive Inkjet Printing. *J. Mater. Chem.* **2009**, *19*, 3719−3724.

(15) Park, B. K.; Kim, D.; Jeong, S.; Moon, J.; Kim, J. S. Direct Writing of Copper Conductive Patterns by Ink-Jet Printing. *Thin Solid Films* **2007**, *515*, 7706−7711.

(16) Grouchko, M.; Kamyshny, A.; Magdassi, S. Formation of Air-Stable Copper-Silver Core-Shell Nanoparticles for Inkjet Printing. *J. Mater. Chem.* **2009**, *19*, 3057−3062.

(17) Luechinger, N. A.; Athanassiou, E. K.; Stark, W. J. Graphene-Stabilized Copper Nanoparticles as an Air-Stable Substitute for Silver and Gold in Low-Cost Ink-Jet Printable Electronics. *Nanotechnology* **2008**, *19*, 445201.

(18) Jang, S.; Seo, Y.; Choi, J.; Kim, T.; Cho, J.; Kim, S.; Kim, D. Sintering of Inkjet Printed Copper Nanoparticles for Flexible Electronics. *Scr. Mater.* **2010**, *62*, 258−261.

(19) Kamyshny, A. Metal-Based Inkjet Inks for Printed Electronics. *Open Appl. Phys. J.* **2011**, *4*, 19−36.

(20) Haynes, W. M. *CRC Handbook of Chemistry and Physics*, 93rd ed; CRC Press: Boca Raton, FL, 2012.

(21) Farnsworth, S.; Schroder, K.; Wenz, B.; Pope, D.; Rawson, I. 32.4: Invited Paper: Broad Implications Arising from Photonic Curing Process For Printed Electronics and Displays. *Dig. Tech. Pap. - Soc. Inf. Disp. Int. Symp.* **2012**, *43*, 430−433.

(22) Dharmadasa, R.; Jha, M.; Amos, D. A.; Druffel, T. Room Temperature Synthesis of a Copper Ink for the Intense Pulsed Light Sintering of Conductive Copper Films. *ACS Appl. Mater. Interfaces* **2013**, *5*, 13227−13234.

(23) Ryu, J.; Kim, H.-S.; Hahn, H. T. Reactive Sintering of Copper Nanoparticles Using Intense Pulsed Light for Printed Electronics. *J. Electron. Mater.* **2011**, *40*, 42−50.

(24) Araki, T.; Sugahara, T.; Jiu, J.; Nagao, S.; Nogi, M.; Koga, H.; Uchida, H.; Shinozaki, K.; Suganuma, K. Cu Salt Ink Formulation for Printed Electronics using Photonic Sintering. *Langmuir* **2013**, *29*, 11192−11197.

(25) Hwang, H.-J.; Chung, W.-H.; Kim, H.-S. In Situ Monitoring of Flash-Light Sintering of Copper Nanoparticle Ink for Printed Electronics. *Nanotechnology* **2012**, *23*, 485205.

(26) Chung, W.-H.; Hwang, H.-J.; Kim, H.-S. Flash Light Sintered Copper Precursor/Nanoparticle Pattern with High Electrical Conductivity and Low Porosity for Printed Electronics. *Thin Solid Films* **2015**, *580*, 61−70.

(27) Kang, H.; Sowade, E.; Baumann, R. R. Direct Intense Pulsed Light Sintering of Inkjet-Printed Copper Oxide Layers within Six Milliseconds. *ACS Appl. Mater. Interfaces* **2014**, *6*, 1682−1687.

(28) Paquet, C.; James, R.; Kell, A. J.; Mozenson, O.; Ferrigno, J.; Lafrenière, S.; Malenfant, P. R. L. Photosintering and Electrical Performance of CuO Nanoparticle Inks. *Org. Electron.* **2014**, *15*, 1836−1842.

(29) Novacentrix Home Page. https://www.novacentrix.com (accessed June 17, 2015).

(30) Kipphan, H. *Handbook of Print Media: Technologies and Production Methods*, 2001 ed; Springer-Verlag: Berlin, Germany, 2001.

(31) Öhlund, T.; Andersson, M. Effect of Paper Properties on Electrical Conductivity and Pattern Definition for Silver Nanoparticle Inkjet Ink. *Proceedings of LOPE-C 2012*, Munich, Germany, June 19−21, 2012; pp 115−119.

(32) Öhlund, T.; Örtegren, J.; Forsberg, S.; Nilsson, H.-E. Paper Surfaces for Metal Nanoparticle Inkjet Printing. *Appl. Surf. Sci.* **2012**, *259*, 731−739.

(33) Bollström, R.; Määttänen, A.; Tobjörk, D.; Ihalainen, P.; Kaihovirta, N.; Österbacka, R.; Peltonen, J.; Toivakka, M. A Multilayer Coated Fiber-Based Substrate Suitable for Printed Functionality. *Org. Electron.* **2009**, *10*, 1020−1023.

(34) Hsieh, M.-C.; Kim, C.; Nogi, M.; Suganuma, K. Electrically Conductive Lines on Cellulose Nanopaper for Flexible Electrical Devices. *Nanoscale* **2013**, *5*, 9289−9295.

(35) Öhlund, T.; Schuppert, A.; Andres, B.; Andersson, H.; Forsberg, S.; Schmidt, W.; Nilsson, H.-E.; Andersson, M.; Zhang, R.; Olin, H. Assisted Sintering of Silver Nanoparticle Inkjet Ink on Paper with Active Coatings. *RSC Adv.* **2015**, *5*, 64841−64849.

(36) Packham, D. Theories of Fundamental Adhesion. In *Handbook of Adhesion Technology*; da Silva, L. M.; Öchsner, A.; Adams, R., Eds.; Springer: Berlin, Heidelberg, 2011; Chapter 2, pp 9−38.

(37) Kim, H.-S.; Dhage, S.; Shim, D.-E.; Hahn, H. T. Intense Pulsed Light Sintering of Copper Nanoink for Printed Electronics. *Appl. Phys. A: Mater. Sci. Process.* **2009**, *97*, 791−798.

(38) Joo, S.-J.; Hwang, H.-J.; Kim, H.-S. Highly Conductive Copper Nano/Microparticles Ink via Flash Light Sintering for Printed Electronics. *Nanotechnology* **2014**, *25*, 265601.

(39) Kim, I.; Joung, J. W.; SONG, Y. A. Reducing Agent for Low Temperature Reducing and Sintering of Copper Nanoparticles, and Method for Low Temperature Sintering Using the Same. Patent US 20100055302, March 4, 2010.

(40) Tobjörk, D.; Aarnio, H.; Pulkkinen, P.; Bollström, R.; Määttänen, A.; Ihalainen, P.; Mäkelä, T.; Peltonen, J.; Toivakka, M.; Tenhu, H.; Österbacka, R. IR-Sintering of Ink-Jet Printed Metal-Nanoparticles on Paper. *Thin Solid Films* **2012**, *520*, 2949−2955.

(41) Gane, P.; Ridgway, C.; Schoelkopf, J.; Bousfield, D. Heat Transfer through Calcium Carbonate-Based Coating Structures: Observation and Model for a Thermal Fusing Process. *J. Pulp Pap. Sci.* **2007**, *33*, 60−70.

DOI: 10.1021/acsami.5b03061
ACS Appl. Mater. Interfaces 2015, 7, 18273−18282

(42) Ha, T.-J.; Park, H.-H.; Kang, E. S.; Shin, S.; Cho, H. H. Variations in Mechanical and Thermal Properties of Mesoporous Alumina Thin Films due to Porosity and Ordered Pore Structure. *J. Colloid Interface Sci.* **2010**, *345*, 120−124.

DOI: 10.1021/acsami.5b03061
ACS Appl. Mater. Interfaces 2015, 7, 18273−18282